# Probabilistic Assessment of Storage Tanks Subjected to Waterborne Debris Impacts during Storm Events

Carl Bernier, A.M.ASCE[1]; and Jamie E. Padgett, A.M.ASCE[2]

**Abstract:** Probabilistic models to evaluate the vulnerability of aboveground storage tanks (ASTs) subjected to waterborne debris impacts during storm surge events are currently lacking, despite evidence of debris-induced damage during past severe storms. This paper addresses a gap in understanding the vulnerability of ASTs subjected to waterborne debris, such as shipping containers, by deriving simulation-based fragility models and an associated risk assessment framework for probabilistic performance assessment. First, finite-element models of ASTs and a shipping container are developed to perform debris impact analyses and assess the potential for damage; the shipping container model is also validated against experimental results. Parametrized fragility models are derived using a statistical sampling method, results of debris impact analyses, and logistic regression. Fragility models are derived for two damage mechanisms: inelastic damage of the tank shell and sliding. Next, this study presents a risk assessment framework to evaluate the probability of an AST being impacted by debris and to demonstrate how the derived fragility models can be employed to evaluate and mitigate the vulnerability of ASTs located in industrial areas. The framework is illustrated for a case study storage tank terminal. Insights obtained from the fragility and risk assessments reveal that large ASTs are less vulnerable than are small ASTs to debris impacts, and that neglecting debris impacts for ASTs located near potential debris sources can significantly underestimate the vulnerability of ASTs during storm surge events. **DOI: 10.1061/(ASCE)WW.1943-5460.0000559**. 

**Author keywords:** Storage tanks; Fragility analysis; Debris impacts; Storm surge; Shipping container; Risk assessment.



## Introduction

Severe hydrodynamic events, such as hurricane storm surge and floods, can generate a massive amount of waterborne debris in coastal regions. Mobile and buoyant objects, such as shipping containers, vehicles, vessels, trees, and wood poles, can become projectiles that impact surrounding structures (Naito et al. 2014; Robertson et al. 2007). Waterborne debris impacts can generate significant loads and thereby cause severe damage to transportation infrastructure and buildings, as well as port and industrial structures (Piran Aghl et al. 2015a). Aboveground storage tanks (ASTs) are one of the commonly damaged industrial structures due to debris impacts. ASTs are typically used in coastal and industrial areas to store large quantities of bulk chemicals, such as oil and gas, and are constructed of thin welded steel plates forming a vertical cylinder. This thin-walled geometry leaves them vulnerable to external loads, such as debris impacts. In fact, following Hurricane Katrina in 2005, the Environmental Protection Agency (EPA) identified waterborne debris impacts as one of the three main causes of AST failures (EPA 2016); AST failures during Katrina caused the spillage of more than 26 million liters of oil products (Godoy 2007). Additional surveys of AST failures during past storm, flood, and tsunami events have also highlighted the potential for damage due to debris impacts (Cozzani et al. 2010; Naito et al. 2013). Debris impacts can typically result in localized damage of the tank shell, potentially rupturing it, as well as sliding of the AST from its foundation, with potential rupture of connected pipes.

AST failures can result in severe environmental and economic impacts due to the spillage of hazardous materials in the environment and social impacts to residential populations living in close proximity to ASTs (Bernier et al. 2017). Consequently, it is critical to assess the structural vulnerability of ASTs during extreme hydrodynamic events. In recent years, several studies (e.g., Kameshwar and Padgett 2018; Landucci et al. 2012) have proposed tools to evaluate the vulnerability of ASTs during storm events. However, these studies have mainly focused on storm surge and wind loads, while neglecting the effects of waterborne debris impacts. Even for other structures than ASTs, few studies have considered the effects of waterborne debris impacts on the vulnerability of coastal structures. The existing literature on waterborne debris has mainly focused on assessing impact loads and debris motion, rather than assessing the behavior and vulnerability of structures subjected to debris impacts (Nistor et al. 2017b; Stolle et al. 2018b). Only a few examples of deterministic debris impact analyses (Como and Mahmoud 2013; Madurapperuma and Wijeyewickrema 2013; Stolle et al. 2019) and empirical fragility curves considering the effects of debris (Charvet et al. 2015; Hatzikyriakou et al. 2016) are currently available in the literature.

This study aims to develop an efficient methodology to evaluate the structural vulnerability of ASTs exposed to waterborne debris during storm events—a method that could also be adapted to other coastal structures exposed to debris. To achieve this objective, this study first derives fragility models for ASTs subjected to waterborne debris impacts by using a simulation-based approach. Fragility models express the probability of damage given a set of structural and hazard parameters and are well-suited tools to address the stochastic nature of debris impact conditions. Fragility models are derived for two potential damage mechanisms under debris impacts: (1) damage to the tank shell; and (2) sliding.

[1]Graduate Research Assistant, Dept. of Civil and Environmental Engineering, Rice Univ., 6100 Main St. MS-318, Houston, 77005 TX. ORCID: https://orcid.org/0000-0002-5207-1973.

[2]Associate Professor, Assistant, Dept. of Civil and Environmental Engineering, Rice Univ., 6100 Main St. MS-318, Houston, 77005 TX (corresponding author). Email: Jamie.Padgett@rice.edu

Note. This manuscript was submitted on March 28, 2019; approved on September 9, 2019; published online on March 16, 2020. Discussion period open until August 17, 2020; separate discussions must be submitted for individual papers. This paper is part of the ***Journal of Waterway, Port, Coastal, and Ocean Engineering***, © ASCE, ISSN 0733-950X.

Then, this study adapts a windborne-debris risk assessment framework to address problems of waterborne debris in industrial and coastal regions, leveraging recent experimental and empirical results for waterborne debris along with the newly derived debris fragility models. As a proof of concept, a scenario-based risk assessment is performed for a case study storage tank terminal located in the Houston, Texas, region. The effectiveness of simple mitigation strategies is also evaluated using this framework.

The fragility models are developed for hydrodynamic conditions representative of tropical storms or hurricanes, given the large concentration of industrial and petrochemical facilities located in hurricane-prone areas along the United States (US) Atlantic and Gulf Coasts and since storm surge has historically been responsible for the most severe AST failures in the US (Sengul et al. 2012). This study focuses on one type of debris: 6.0-m (20-ft) ISO shipping containers. Shipping containers are considered since they are one of the most common type of debris in industrial regions, where ASTs are also located, and given the availability of experimental and empirical results to characterize motions and impact conditions for this type of debris (e.g., Derschum et al. 2018; Naito et al. 2014; Piran Aghl et al. 2014; Riggs et al. 2014; Stolle et al. 2018b), providing useful insights for this study.

The next sections of this paper detail the approach to develop fragility models and assess the risks posed to ASTs by waterborne debris during storms. First, this study presents the development and validation of finite-element (FE) models of ASTs and shipping containers to perform debris impact analysis and assess the potential for damage. Then, the ranges of modeling parameters, storm surge conditions, and debris impacts conditions considered for the fragility analysis are defined. Next, the fragility assessment methodology is presented, and parametrized fragility models are derived using the FE models, a statistical sampling method, and logistic regression. The risk assessment framework is then presented and illustrated for a case study region; the viability of procedural mitigation strategies to reduce risks is also discussed. Finally, a discussion on the limitations of the present study and future research opportunities is presented.

## Finite-Element Modeling of Debris Impacts

The development of fragility models requires an adequate estimation of the demand imposed by waterborne debris and the performance of ASTs under debris impacts. Due to a lack of empirical data regarding the performance of ASTs during storms, this study relies on numerical methods to evaluate both the debris impact loads and the structural behavior of ASTs; two FE models, one for ASTs and one for 20-ft (6.0-m) ISO shipping containers, are developed and then coupled to perform debris impact simulations.

### *Aboveground Storage Tanks*

This study only focuses on ASTs with a fixed conical roof supported by rafters and columns as they are one of the most common types of ASTs along the US Atlantic and Gulf Coasts (Bernier 2019); however, the methodology presented here can be adapted for any type of AST or roof. Fig. 1 presents an example, a schema, and the details of a conical roof AST. First, for an AST with a given geometry [i.e., diameter ($D$) and height ($H$)] and design stress ($S_d$) value, the number of shell courses, the thickness of each course, the presence of stiffening rings, and the roof properties are determined in accordance with the American Petroleum Institute (API) Standard 650 (API 2013). Then, the AST is modeled in *LS-Dyna*, a commercial finite-element software; Fig. 1(d) presents an overview of the FE model. In *LS-Dyna*, the shell courses are modeled with fully integrated quadrilateral shell elements, the roof with reduced integration triangular shell elements, and the stiffening ring and roof rafters with beam elements. At the base of the AST, the translational degrees of freedom (DOFs) are fixed, while the rotational DOFs are free. The mesh size of the shell course is fixed at approximately 0.25 m, based on conducting mesh convergence studies of ASTs with various geometries and using the debris impact analysis methodology detailed later. Beyond the mesh sensitivity study, no other validation of the FE model is performed, given the lack of empirical or experimental data regarding the structural behavior

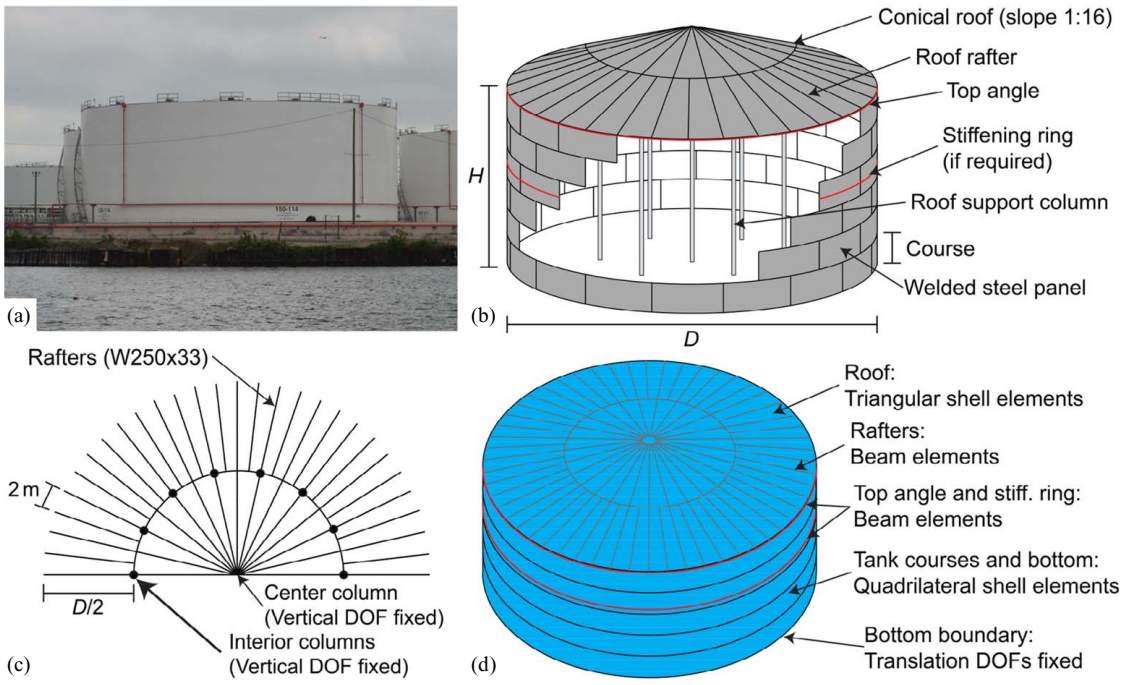


**Fig. 1.** (a) Example of a conical roof AST in the Houston region ($D = 45$ m; $H = 16$ m; image by Carl Bernier); (b) schema of a typical conical roof AST; (c) details of a conical roof; and (d) finite-element representation of a conical roof AST.



J. Waterway, Port, Coastal, Ocean Eng., 2020, 146(3): 04020003

of ASTs during storm events. A bilinear elastoplastic material model with kinematic hardening and the physical properties of steel is assigned to all components. The steel density is fixed at 7,900 kg/m$^3$, the elastic modulus at 200 GPa, the Poisson's ratio at 0.3, and the tangent modulus after yielding at 2 GPa, while the yield strength is a function of $S_d$ (API 2013). Strain rate effects are considered using the Cowper-Symonds model with the parameters proposed by Cowper and Symonds (1957), which are representative of steel grades like the ones used for ASTs. A damping ratio of 2%, representative of undamaged welded steel (Paultre 2011) is assigned to all components. Finally, geometric imperfections of the tank shell are considered as they can significantly affect the structural behavior. Using the imperfection model proposed by Kameshwar and Padgett (2016), the imperfections are modeled using a two-dimensional Fourier series with random coefficients derived from empirical measurements of imperfections on ASTs and silos.

### Shipping Container

An adequate estimation of the loads imposed by shipping containers is required in order to perform debris impact analysis with the above FE model of ASTs. In recent years, several studies have proposed analytical models to estimate waterborne debris impact loads. However, while these existing debris load models might be adequate for design purposes, they are not appropriate for fragility or performance assessments, since typically they use major assumptions that can introduce significant uncertainties and result in overly conservative load estimates (Madurapperuma and Wijeyewickrema 2013; Stolle et al. 2018a); these assumptions relate to the debris properties and behavior, the effects of debris orientation and eccentricity, the impact duration, and the contact area of the debris impact. Therefore, to adequately evaluate the demand imposed on ASTs, this study develops and validates a high-fidelity FE model of a 20-ft ISO shipping container.

Fig. 2 presents an overview of the 20-ft shipping container FE model. The model is developed in *LS-Dyna* and comprises all the main structural components. The shipping container has a length of 6.1 m, a width of 2.4 m, a height of 2.6 m, and a tare mass of 2,100 kg. The exact dimensions and specifications of each of the components were obtained from a shipping container manufacturer (Containex 2013). All components are modeled using reduced integration quadrilateral shell elements; a maximum mesh size of 0.05 m is adopted. With the exception of the plywood floor, all components are assigned with an elastoplastic material model with kinematic hardening and the steel properties proposed by Piran Aghl et al. (2015a), which are based on coupon tests from an actual 20-ft shipping container. The steel density is fixed at 7,800 kg/m$^3$, the elastic modulus at 207 GPa, the Poison ratio at 0.3, the tangent modulus after yielding at 0.5 GPa, and the yield strength at 381 MPa. Strain rate effects are considered using the same model and parameters as for the AST (Madurapperuma and Wijeyewickrema 2013). The plywood floor is modeled using an elastic material with a density of 750 kg/m$^3$, elastic modulus of 5 GPa, and Poisson's ratio of 0.3. A general surface-to-surface contact is defined to model the internal contact between the different components of the container when large deformation occurs. Finally, the nonstructural mass ($m_d$) of the container (i.e., the mass of the contents) is modeled as lumped masses that are rigidly tied to the plywood floor. While rigidly attaching the nonstructural mass might result in conservative impact forces (Piran Aghl et al. 2015b), this assumption is employed given the large uncertainties regarding the actual connectivity between the nonstructural mass and the shipping containers.

To ensure an adequate response of the shipping container, the FE model is validated against a series a full-scale in-air shipping container impact tests performed at Lehigh University by Piran Aghl et al. (2014). During their experiments, impacts were generated by attaching a shipping container to a pendulum system and the impact forces were recorded using load cells. Different configurations of load cells and impact velocities were employed to evaluate elastic and inelastic impacts of a single corner and multiple corners of a shipping container. More details on the experiments can be found in Piran Aghl et al. (2014). To perform the validation, the load cells used during the experiments are modeled in *LS-Dyna* using the recommendations presented in Piran Aghl et al. (2015a). A surface-to-surface contact between the load cells and the shipping container is then defined; a Coulomb friction coefficient of 0.21 is used for the contact. Finally, an initial velocity equal to the impact velocity measured during the experiments is assigned to the shipping container and the impact force time history between the container and the load cell is recorded. Fig. 3 presents the comparison between the FE model and the experiment for eight different impact cases. Fig. 3(a) presents the three and four corners impacts, Fig. 3(b) the one and two bottom corners impacts, and Fig. 3(c) the one and two top corners impacts. Impacts with a velocity of 1.5 m/s result in elastic impacts, while those with a velocity of 3.8 m/s in inelastic impacts; in all

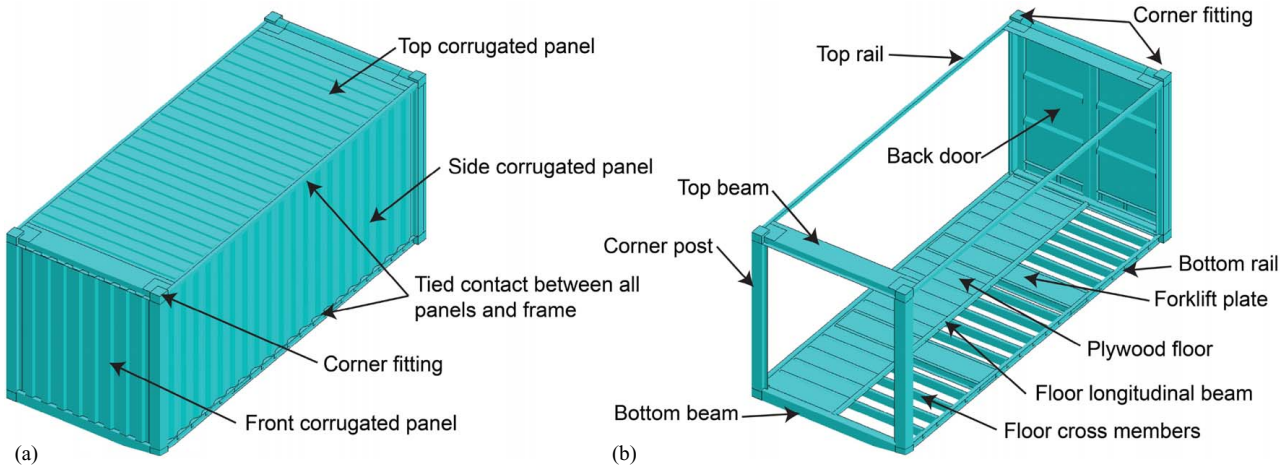


**Fig. 2.** Shipping container finite-element model: (a) general overview; and (b) details of structural frame.



J. Waterway, Port, Coastal, Ocean Eng., 2020, 146(3): 04020003

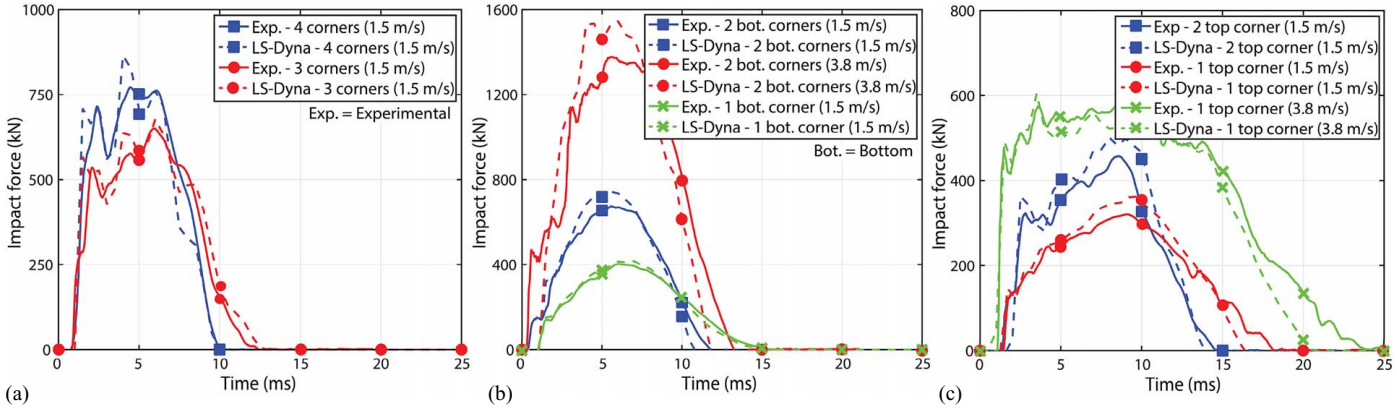


**Fig. 3.** Comparison between the *LS-Dyna* FE model and experimental results for different impact cases: (a) three or four corners impacts; (b) bottom corners impacts; and (c) top corners impacts. (Experimental data from Piran Aghl et al. 2014.)

cases the shipping container is empty (i.e., $m_d = 0$ kg). Overall, the results presented in Fig. 3 indicate a good agreement between the FE model and the experiments. For the impact forces ($F_d$), the FE model overestimates the experimental results by 4%–12%, while for the impact duration ($t_d$), the FE model underestimates the experimental results by 0%–13%. This comparison indicates that the shipping container FE model can be confidently employed to perform the debris impact analysis detailed in the next subsection.

### Debris Impact Analysis

With the two FE models presented previously, it is now possible to evaluate the structural behavior of ASTs subjected to shipping container impacts. Fig. 4 summarizes the different parameters defining the debris impact analysis. The impact conditions are defined by the surge height ($S$), the debris nonstructural mass ($m_d$), the debris orientation in the horizontal ($\alpha$) and vertical ($\beta$) planes, the debris eccentricity with respect to the AST center ($y_d$), and the debris velocity ($U_d$). As explained below, the debris velocity is considered independent from the water velocity ($U_w$) for more flexibility, although their correlation could be considered in subsequent risk analyses. To perform the impact analysis, the shipping container FE model is imported in the AST FE model. The shipping container is then oriented and located appropriately based on $\alpha$, $\beta$, $x_d$, $y_d$, and $z_d$, as show in Fig. 4; $z_d$ is obtained from buoyancy calculations given $S$ and $m_d$, while $x_d$ is defined such that the impact occurs at approximately 1 s during the analysis. As for the validation analyses, a surface-to-surface contact is defined between the shipping container and the AST, and an initial velocity equal to $U_d$ is assigned to the shipping container. The impact analysis is performed using the explicit solver in *LS-Dyna,* and the resultant reaction force at the base of the AST as well as the tank shell displacement ($\Delta$) time histories at the impact location are recorded. As detailed in the next section, the resultant reaction forces are used to assess sliding, while the tank shell displacements are used to assess damage to the tank shell.

When performing the impact analysis, the gravity loads, internal pressures from the AST contents, and external pressures from the storm surge are also applied on the AST tank shell. Both the hydrostatic pressure of the surge, defined by $S$ and the sea water density ($\rho_w$), and the AST internal liquid pressure, defined by the internal liquid height ($L$) and the internal liquid density ($\rho_L$), are modeled using triangular pressure distributions. The hydrodynamic pressure of the surge (i.e., current and wave loads) is applied on the AST

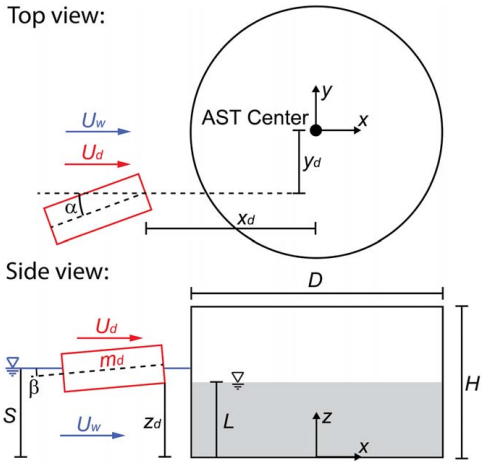


**Fig. 4.** Definition of debris impact parameters.

using the load model presented in Bernier and Padgett (2019). This load model was derived from experimentally validated computational fluid dynamic analyses and provides the hydrodynamic pressure distributions around ASTs as a function of the diameter ($D$), surge height ($S$), current velocity ($U_w$), wave height ($H_w$), and wave period ($T_w$). While the effects of hydrodynamic loads on the AST are considered, the effects of these hydrodynamic loads on the debris (i.e., added mass) are not considered here. It is acknowledged that neglecting these effects might significantly affect impact loads on ASTs (Shafiei et al. 2016). However, the estimation and modeling of added mass effects pose significant challenges, requiring further research, given the complexity and uncertainties associated with these effects (Nistor et al. 2017b; Stolle et al. 2018a).

Fig. 5 presents an example of debris impact time histories and-displacement contours for $D = 15$ m, $H = 10$ m, $L = 5$ m, $S = 3.0$ m, $\rho_L = 750$ kg/m$^3$, $m_d = 10{,}000$ kg, $U_d = U_w = 1.5$ m/s, $\alpha = \beta = 0°$, $y_d = 3.5$ m, and $H_w = T_w = 0$. In this figure, Node A is at the impact location, which corresponds to the bottom-left corner of the shipping container, while Node B is located 2 m away from the impact location. As observed in this figure, the AST suffers inelastic damage since there is a 20 mm residual displacement following the impact. It is also possible to observe that the deformations and inelastic behavior of the tank shell are highly localized at the impact location, displacements at Node B being significantly smaller than the ones at Node A.

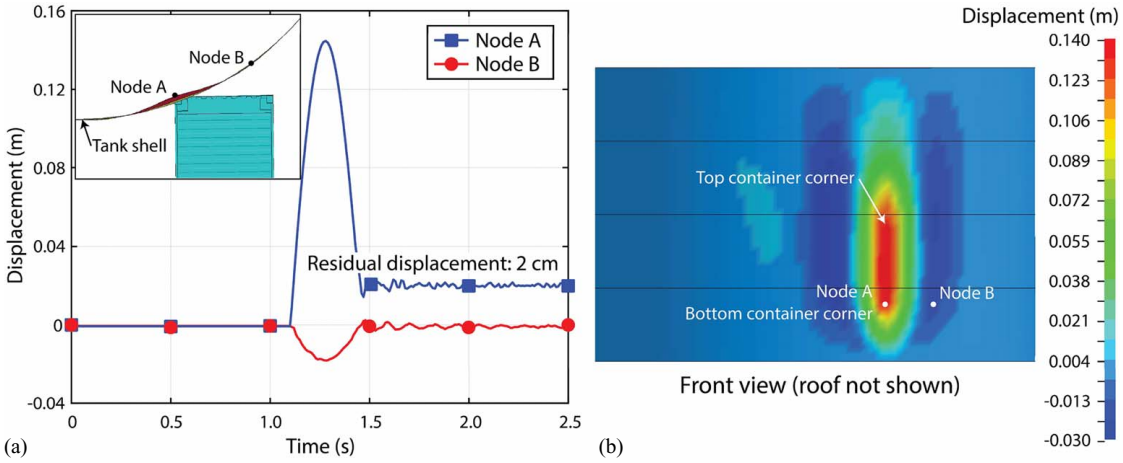


**Fig. 5.** (a) Displacement time histories; and (b) displacement contours at impact for $D = 15$ m, $H = 10$ m, $L = 5$ m, $S = 3.0$ m, $\rho_L = 750$ kg/m$^3$, $m_d =$ 10,000 kg, $U_d = 1.5$ m/s, $\alpha = \beta = 0°$, and $y_d = 3.5$ m.

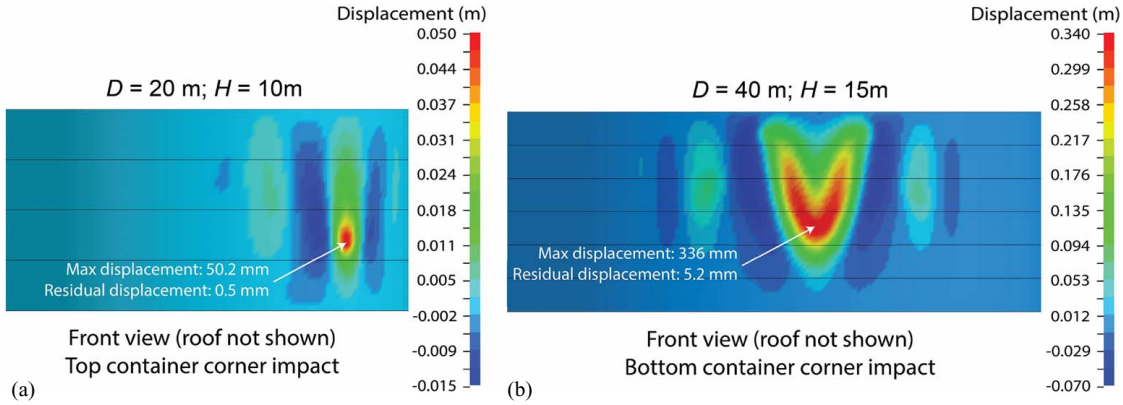


**Fig. 6.** Displacement contours at impact for: (a) $D = 20$ m, $H = 10$ m, $S = 2.0$ m, $L = 5$ m, $\rho_L = 750$ kg/m$^3$, $m_d = 14{,}000$ kg, $U_d = 2.0$ m/s, $\alpha = -20°$, $\beta = -5°$, and $y_d = 8.0$ m; and (b) $D = 40$ m, $H = 15$ m, $S = 7.0$ m, $L = 7$ m, $\rho_L = 750$ kg/m$^3$, $m_d = 14{,}000$ kg, $U_d = 2.0$ m/s, $\alpha = 20°$, $\beta = 5°$, and $y_d = 2.0$ m.

## Damage Mechanisms

With the results of a debris impact analysis for a given AST and a given set of surge and debris impact conditions, the potential for damage can be assessed. Damage to the AST tank shell is one of the two damage mechanisms considered here. Severe inelastic damage can lead to the rupture of the tank shell and the release of the internal liquid (i.e., loss of containment). As previously observed in Fig. 5, severe displacements and inelastic damage almost always occur at the impact location. Additional impact cases shown in Fig. 6 further confirm this damage pattern. Thus, by adopting an approach similar to the one proposed by Herbin and Barbato (2012), the potential for damage to the tank shell is determined from the residual inelastic displacement ($\Delta_{pl}$) at the impact location. The condition of tank shell damage is assessed using the limit state function shown in the following equation; damage occurs if the limit state function is below zero:

$$g_{\text{damage}} = \Delta_{pl} - \zeta_{pl} \tag{1}$$

where $\zeta_{pl}$ = a residual displacement threshold. Since there is currently limited information regarding the displacement thresholds that should be adopted for ASTs, two thresholds of increasing magnitude are assumed here. The first threshold corresponds to the initiation of inelastic behavior (i.e., $\zeta_{pl1} = 0$ mm), while the second one corresponds to a residual displacement of $\zeta_{pl2} = 25$ mm (1 in.). It is acknowledged that these thresholds do not indicate the actual failure (i.e., rupture or perforation) of the tank shell or the loss of containment, and that future research is required to define more comprehensive thresholds. Nonetheless, the two damage levels adopted here can provide useful insights regarding the severity of an impact and the magnitude of inelastic damage.

The second damage mechanism investigated is sliding, which can potentially lead to the rupture of connected pipes and valves. The potential for sliding is assessed by evaluating the two following limit state functions. Sliding occurs if either of the following is below zero:

$$g_{\text{sliding1}} = (W_t + W_L - F_b) \cdot \varphi - R \tag{2}$$

$$g_{\text{sliding2}} = ((W_t + W_L - F_b) \cdot \varphi) \cdot D/2 - R \cdot (D/2 + y_R) \tag{3}$$

where $W_t$ = the tank weight, which can be estimated once the tank thickness and roof design is determined per the API 650 Standard; $W_L = \pi g \rho_L L D^2/4$ = the internal liquid weight; $F_b = \pi g \rho_w S D^2/4$ = the buoyant force from the surge; $\varphi$ = the friction coefficient at the AST foundation; $R$ = the maximum resultant reaction force at

the base of the AST recorded during the debris impact analysis; and $y_R$ = the location of the resultant reaction with respect to the AST center. Eq. (2) considers the case where sliding occurs in the $x$ direction, whereas Eq. (3) considers the case where rotation around the $z$ axis occurs due to the debris eccentricity. Again, Eqs. (2) and (3) only indicate whether sliding occurs or not and do not provide any information regarding the potential for a loss of containment. Both equations are derived from sums of forces and moments and assume that the AST bottom plate behaves rigidly during a debris impact. This assumption was validated by performing preliminary analyses with the model presented in Fig. 1, for which the contact between the bottom plate and the foundation is modeled using a surface-to-surface contact with a Coulomb friction coefficient equal to $\varphi$ rather than fixing the translational DOFs. The impact force time history was then applied at the impact location. Given the localized nature of debris impacts, no significant uplift or deformations of the tank bottom plate were observed, allowing the simple use of Eqs. (2) and (3) instead of more-complex FE analysis to evaluate sliding. For anchored ASTs, the shear strength of the anchors (Eligehausen et al. 2006) should be included in Eqs. (2) and (3). However, only unanchored ASTs are considered here since sliding is not a critical failure mode for anchored ASTs and the ranges of debris impact and hydrodynamic conditions considered in the next section. The shear strength provided by anchors would be well in excess of the reaction force at the base of ASTs. Moreover, it is not a common design practice to anchor ASTs in typical storm surge-prone regions in the US, such as the Gulf Coast (Bernier et al. 2017). Nonetheless, under more severe hydrodynamic conditions, such as tsunamis, sliding might become critical for anchored ASTs, and future research looking at regions with anchored ASTs should consider this possibility.

## Storm and Debris Impact Conditions

To conduct the fragility assessment, the performance of ASTs must be evaluated for numerous combinations of hydrodynamic conditions, debris impact conditions, and AST modeling parameters. Thus, a careful definition of the ranges of storm, debris, and modeling parameters is required. Table 1 presents the range of storm conditions considered in the fragility analysis. Due to a lack of empirical data for industrial locations, these ranges are obtained from numerical simulations of hurricanes in and around the Houston region in Texas. The Computational Hydraulics Group at the University of Texas at Austin performed the simulations using *ADCIRC + SWAN* by for Hurricane Ike, which made landfall in the Houston region in 2008, and for two synthetic storms developed by FEMA, which correspond to approximately 100- and 500-year storm surge events in the Houston region (Ebersole et al. 2016); the synthetic storms are commonly referred to as storm FEMA033 and FEMA036, respectively. Hydrodynamic conditions (i.e., $S$, $U_w$, $H_w$, and $T_w$) were extracted at several industrial sites in the Houston region to obtain the ranges shown Table 1. Even though *ADCIRC + SWAN* has not been extensively validated for onshore locations, especially for current and wave conditions, *ADCIRC + SWAN* results are employed here given the lack of other models to estimate hydrodynamic conditions at AST locations during severe storm events. Nonetheless, as a sanity check, the extracted surge conditions were compared against empirical relations found in USACE (2008). Lastly, the lower limit of $S$ is adjusted to 1.0 m, since it is unlikely that ASTs would be subjected to lower water levels due to the presence of containment berms; by regulations, ASTs are protected by berms and the height of these berms is typically higher than 1.0 m (Bernier et al. 2017). This limit also corresponds to the one proposed by Naito et al. (2014) to determine if debris would be grounded or not. Furthermore, the AST hydrodynamic load model employed in this study is not valid for surge heights lower than 1.0 m. The use of this load model also requires that the ratio $H_w/S$ is lower than 0.65 (Bernier and Padgett 2019).

Table 2 summarized the ranges of debris impact conditions considered in the fragility analysis. The upper bound for $m_d$ is defined by subtracting the tare weight (2,100 kg) of the shipping container from the maximum gross weight (30,400 kg). As shown in Table 2, the upper bound of the nonstructural mass is also limited to ensure that the debris would be buoyant given $S$; $m_b$ is the maximum allowable nonstructural mass for which a shipping container can be buoyant for a given surge height. As explained in the previous section, $U_d$ is assumed to be independent from $U_w$ for the statistical sampling of parameters for fragility development, and a wider range of velocity is considered for the debris. The upper bound of $y_d$ is limited by the AST geometry. Lastly, $\alpha$ and $\beta$ are limited to $\pm 45°$ and $\pm 10°$ in order to consider impacts in the longitudinal axis of the container since (1) the validation of container FE model is limited to longitudinal impacts; and (2) preliminary analyses indicated that impacts with $|\alpha| < 45°$ induced significantly more severe deformations of the tank shell than impacts with $|\alpha| > 45°$.

Finally, Table 3 details the ranges of AST modeling parameters considered in the fragility analysis. The ranges of geometry (i.e., $D$ and $H$) and internal liquid properties (i.e., $L$ and $\rho_L$) are obtained from the comprehensive database of ASTs developed in Bernier et al. (2017). The lower bound of the internal liquid height is adjusted such that damage due to storm surge loads alone is avoided (i.e., flotation and storm surge buckling) and that damage occurs uniquely due to debris impacts or interactions between surge

**Table 1.** Ranges of storm conditions considered in the fragility analysis

| Parameter | Lower bound | Upper bound | Units |
|---|---|---|---|
| Surge height ($S$) | 1.0 | 7.0 | m |
| Current velocity ($U_w$) | 0.2 | 1.5 | m/s |
| Wave height ($H_w$) | 0.2 | max(2.0; 0.65$S$) | m |
| Wave period ($T_w$) | 3.0 | 6.0 | s |

**Table 2.** Ranges of debris impact conditions considered in the fragility analysis

| Parameter | Lower bound | Upper bound | Units |
|---|---|---|---|
| Nonstructural mass ($m_d$) | 0 | max(28,300; $m_b$) | kg |
| Debris velocity ($U_d$) | 0.2 | 2.5 | m/s |
| Debris eccentricity with respect to the AST center ($y_d$) | 0.0 | 0.5$D$ | m |
| Angle between debris axis and velocity direction ($\alpha$) | −45 | 45 | ° |
| Angle between debris axis and water surface ($\beta$) | −10 | 10 | ° |

**Table 3.** Ranges of AST modeling parameters considered in the fragility analysis

| Parameter | Lower bound | Upper bound | Units |
|---|---|---|---|
| Diameter ($D$) | 5.0 | 60.0 | m |
| Relative height ($H/D$) | $\exp((1-2\ln D)/4)$ | $\exp(3-0.95\ln D)$ | — |
| Internal liquid relative density ($\rho_L$) | 0.5 | 1.0 | — |
| Internal liquid height ($L$) | $S/\rho_L$ | 0.9$H$ | m |
| Design stress ($S_d$) | 137 | 196 | MPa |
| Coefficient of friction ($\varphi$) | 0.3 | 0.7 | — |

loads and debris impacts; the minimum value for $L$ is estimated as $S/\rho_L$ based on the fragility analysis of Bernier (2019) for ASTs subjected to storm surge only. Thus, the fragility models developed in the next section do not consider the potential for damage mechanisms other than the ones related to debris impacts. This assumption is adequate since debris impacts are commonly considered as the last possible cause of damage for ASTs not already damaged by surge or flood loads (Krausmann and Mushtaq 2008). Finally, for $S_d$, which defines the AST thickness and yield strength, the range is obtained from the API 650 Standard (API 2013), while for $\varphi$, the range is obtained from Leonards (1965) and Rabbat and Russell (1985) and covers foundation materials such as concrete, grout, sand, and gravel.

## Fragility Assessment

With FE models, knowledge of the damage mechanisms and the ranges of load and modeling parameters, the fragility assessment is subsequently performed. This study develops simulation-based and parameterized fragility models, which provide the probability of damage as a function of the set of surge parameters ($\boldsymbol{IM_S} = \{S, U_w, H_w, T_w\}$), the set of debris parameters ($\boldsymbol{IM_D} = \{m_d, U_d, y_d, \alpha, \beta\}$), and the set of AST parameters ($\boldsymbol{X} = \{D, H, L, \rho_L, S_d, \varphi\}$). Such parametrized fragility models are useful tools to propagate sources of uncertainty when evaluating the vulnerability of an AST.

To derive the fragility models, Latin Hypercube Sampling (LHS) (Mckay et al. 1979) is first employed to generate simulation samples that efficiently span the space of storm, debris, and AST parameters presented in Tables 1–3. For each sample, which corresponds to a different combination of parameters, a debris impact analysis is performed and the maximum residual displacement ($\Delta_{pl}$) and resultant reaction force ($R$) are extracted. Then, for each sample, the limit state functions—Eq. (1) for damage to the tank shell and Eqs. (2) and (3) for sliding—are evaluated to determine if the AST survived (0) or failed (1). Next, the samples are divided in a training set (90%) and a test set (10%), and, using the binary output of the training samples, the fragility models are derived using logistic regression, as

$$P(\text{Damage}|\boldsymbol{IM_S}, \boldsymbol{IM_D}, \boldsymbol{X}) = \frac{1}{1 + \exp\left(-l(\boldsymbol{IM_S}, \boldsymbol{IM_D}, \boldsymbol{X})\right)} \quad (4)$$

Separate fragility models are derived for damage to the tank shell and sliding. In the above equation, $l(\boldsymbol{IM_S}, \boldsymbol{IM_D}, \boldsymbol{X})$ is a logit function that expresses the log-odds of damage. The logit function is obtained through stepwise regression such that only the most influential storm, debris, and AST parameters or polynomial combinations of parameters are considered. The logit functions for the different fragility models derived in the next subsections can be found in the Supplemental Materials; Table S1 presents an overview of the variables of the logit functions. Finally, the accuracy of the logistic classifier is assessed using the test samples. Since the fragility models are both developed and tested using numerical simulations, the models might be affected by large epistemic uncertainties associated with the modeling assumptions and the limited validation of the numerical models. The accuracy, as computed here, does not capture the effects of such uncertainties on the performance and adequacy of the fragility models.

### Damage to the Tank Shell

The first fragility models developed here are for damage to the tank shell. A total of 1,000 samples were generated to derive the fragility model, 900 for training and 100 for testing. Debris impact analyses were performed for the 1,000 samples to determine $\Delta_{pl}$, and Eq. (1) was then used to assess if damage occurs or not. Separate fragility models are developed for the two displacement thresholds (i.e., $\zeta_{pl1} = 0$ and $\zeta_{pl2} = 25$ mm). The logit functions obtained with the training samples are presented in Tables S2 and S3 in the Supplemental Materials for $\zeta_{pl1} = 0$ and $\zeta_{pl2} = 25$ mm, respectively. On the test samples, the accuracy of the fragility models is of 92.0% and 94.0%, respectively, indicating a good fit of the models against the numerical simulations. The use of the fragility models requires knowledge of all the parameters listed in Tables 1–3. However, if some parameters are uncertain, it is possible to convolve Eq. (4) over the probability density functions (PDFs) of the uncertain parameters using numerical integration in order to condition the fragility models on a smaller set of parameters. This approach was employed to obtain the fragility curves shown in Fig. 7 for two case study ASTs; Tank A ($D = 15$ m and $H = 10$ m) is a small size AST, while Tank B ($D = 40$ m and $H = 15$ m) is a large size AST according to the AST database in Bernier et al. (2017). In this figure, the fragility models are only conditioned on $U_d$; $D$, $H$, and $m_d$ are fixed to the value shown in the figure, while $S_d = 160$ MPa, $S = 6$ m, $L = 4$ m, $\rho_L = 750$ kg/m$^3$, $U_w = 0.75$ m/s, $H_w = 1.0$ m, and $T_w = 4.0$ s; and $\alpha$, $\beta$, and $y_d$ are assumed to be uniformly distributed with the bounds in Table 2.

Fragility curves such as the ones presented in Fig. 7 provide useful insights regarding the structural vulnerability of ASTs subjected to waterborne debris impacts. Fig. 7 indicates that small ASTs are more vulnerable to debris impacts than are large ASTs. For an impact velocity of 2.5 m/s, the probability of suffering damage due to an empty container ($m_d = 0$ kg) is less than 0.15 for Tank B, and is higher than 0.8 for Tank A. The same trend is also observed for a full container ($m_d = 28{,}300$ kg) impact and is due to the fact that the tank shell thickness increases as the tank diameter increases. As expected, Fig. 7 also highlights the large influence of the debris nonstructural mass on the probability of damage. For both ASTs, the likelihood of inelastic damage is significantly higher when a full shipping container impact is considered. Also, for an empty container, the probability of having a residual displacement larger than 25 mm is null for the range of velocity considered here for both ASTs. However, for a full container impact, the probability of $\Delta_{pl} > 25$ mm quickly approaches 1.0 for Tank A, while it can reach a value up to 0.8 for Tank B. To better understand the influence of the debris impact conditions on the likelihood of damage, a series of additional debris impact analyses were performed; the results are presented in Fig. 8. This figure illustrates how varying one impact parameter at a time, from their lower to upper level in Tables 1 and 2, affects the magnitude of the inelastic damage for Tanks A and B; when varying a parameter, all others are kept at their median values. Results indicate that across the parameter ranges considered, $m_d$ and $U_d$ have the largest influence on the potential for damage. Increasing $S$ reduces the likelihood of damage as the tank shell is more flexible at the impact location. Impacts with $y_d$ values close to 0 are more likely to induce damage. For $y_d$ close to $0.5D$, the debris bounces off the tank shell with limited damage. For large ASTs, an impact with $y_d$ close to $0.5D$ will not induce any damage, explaining why the probability of damage of Tank B never reaches 1.0 in Fig 7(b). As shown in Fig. 8, the orientation of the shipping container also plays a significant role. The value of $\alpha$ determines how the shipping container bounces off; impacts with $\alpha > 0°$ reduce the likelihood of damage, compared with cases with $\alpha < 0°$, which increase it. Finally, the value of $\beta$ determines if a top or bottom corner of the shipping container will impact first. Since bottom corners have a larger stiffness, values of $\beta > 0°$ yield are more likely to induce damage.

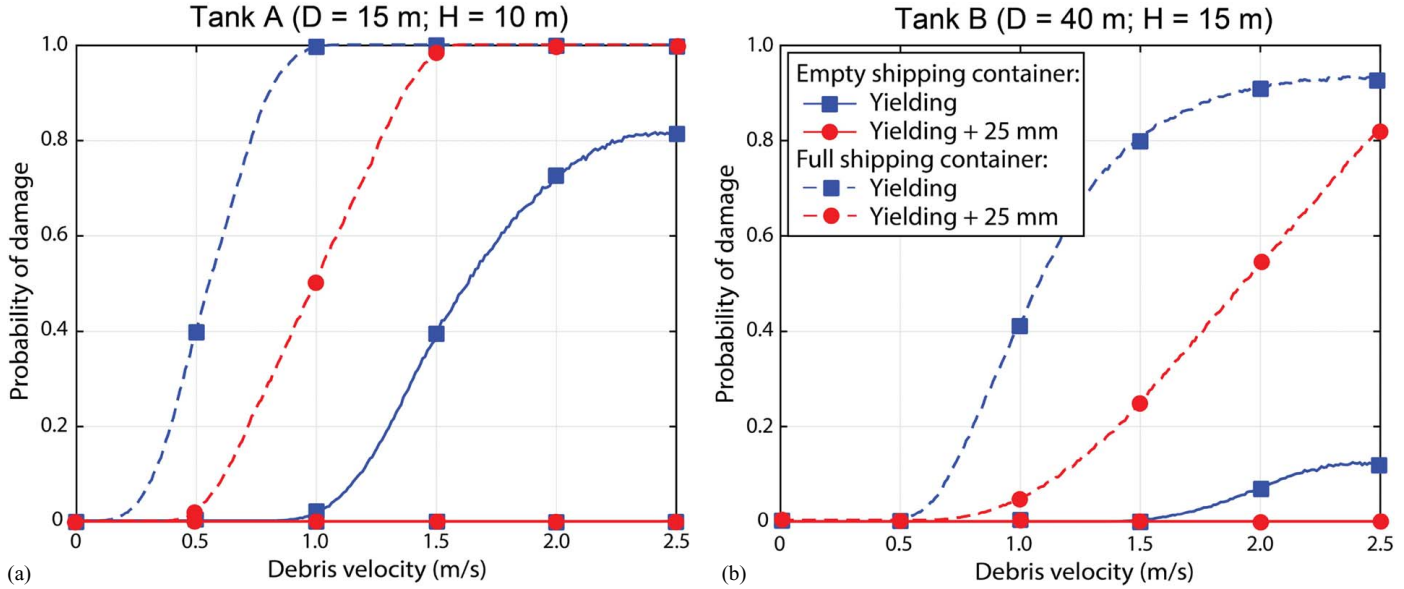


**Fig. 7.** Tank shell damage fragility curves for: (a) Tank A; and (b) Tank B.

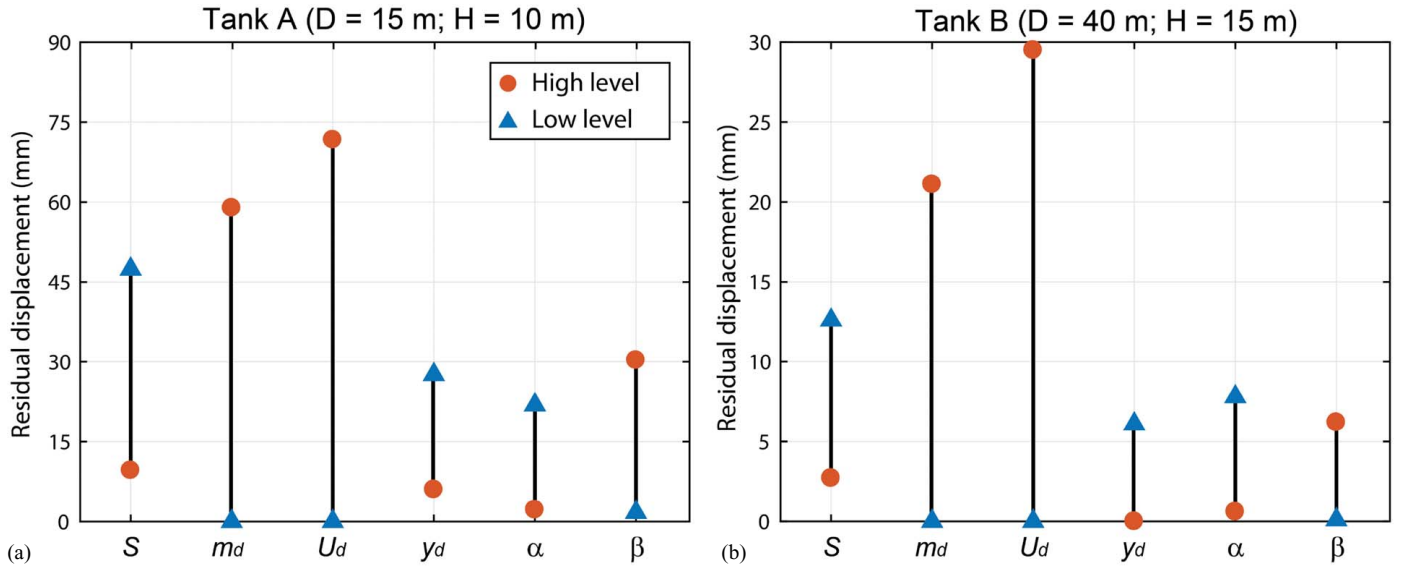


**Fig. 8.** Effects of varying debris impact parameters on inelastic damage for: (a) Tank A; and (b) Tank B.

### *Sliding of the AST*

A third fragility model is also developed for the sliding of ASTs due to debris impacts. The sliding fragility model was derived using the same 1,000 samples generated for the tank shell damage fragility models. For each sample, the maximum resultant reaction force at the base of the AST ($R$) was extracted from the debris impact analysis, and Eqs. (2) and (3) were then evaluated to assess whether sliding occurs or not. Table S4 in the Supplemental Materials presents the logit function obtained with the training samples. The accuracy of the sliding fragility model on the test samples is 98.0%, which indicates again a good fit of the classifier against the numerical simulations. Fig. 9 illustrates the probability of sliding of Tanks A and B. This figure was generated using the same methodology as Fig. 7; all parameter values are identical, with the addition of $\varphi = 0.5$. Fig. 9 indicates that the probability of sliding is null for Tank B, given the large surface between the AST bottom and the foundation to resist sliding, as well as for empty shipping container impacts, given the small impact force in such case. However, for Tank A and a full shipping container, the probability of sliding can reach a value of almost 0.95. By comparing Figs. 7 and 9, it appears that damage to the tank shell is the most critical and likely damage mechanism for ASTs subjected to waterborne debris. In most cases, the probability of damage to the tank shell is always higher than the probability of sliding. The probability of sliding is only higher when small ASTs ($D < 10$ m) with a low friction coefficient are subjected to shipping containers with a large nonstructural mass. Lastly, the trends observed regarding the influence of the debris impact conditions (i.e., $S$, $y_d$, $\alpha$, and $\beta$) on the probability of sliding are similar to the ones observed for tank shell damage.

Overall, the results presented in Figs. 7 and 9 indicate that for practical ranges of debris velocity and mass, shipping container impacts can result in AST damage. Depending on the impact conditions, significantly high probabilities of damage to the tank shell or of sliding are observed. Given the serious consequences of

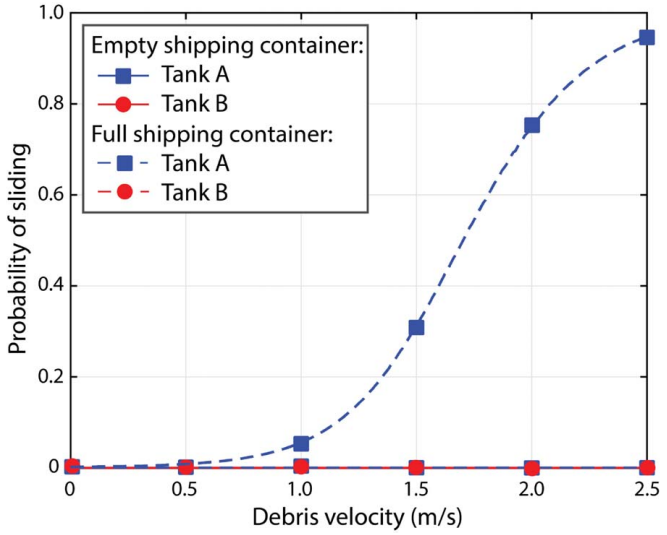


**Fig. 9.** Sliding fragility curves for Tanks A and B.

AST failure, such results highlight the fact that waterborne debris impacts should be considered when assessing the structural vulnerability of ASTs during storm surge events. The parameterization of the derived models also enables the estimation of the potential for damage for any reasonable AST geometry, internal liquid properties, storm surge conditions, and debris impact conditions, facilitating risk assessments as detailed in the next section.

## Risk Assessment

Even though these fragility models are useful tools to evaluate the structural vulnerability of ASTs subjected to waterborne debris impacts, they only provide the probability of damage if a debris impact occurs. To perform comprehensive vulnerability and risk assessments, the probability of an AST being hit by waterborne shipping containers must also be evaluated. Thus, this section presents a risk assessment framework to evaluate the probability of being hit by debris and then the potential for AST damage during a storm surge event. As a proof of concept, the framework is illustrated for a case study area. To provide further insights, the framework is also employed to evaluate the viability of mitigation strategies.

### *Probability of Debris Impacts and Damage*

To evaluate the probability of being hit by debris during a storm surge event, this study adapts the risk assessment framework for windborne debris proposed by Lin and Vanmarcke (2010) for use in coastal regions with waterborne debris, incorporating insights from recent experimental and empirical results for waterborne debris presented in Naito et al. (2014) and Stolle et al. (2018b, c) along with the fragilities derived in this paper. Even though the studies of Naito et al. (2014) and Stolle et al. (2018b) focus on waterborne debris during tsunami events, given the lack of data for debris during storm surge events, their results on debris motion and spreading are employed here. Moreover, since these studies tend to focus on idealized flow conditions, the proposed framework might not capture all the complexities associated with debris motions and impacts during an actual storm event.

Fig. 10 illustrates the method to estimate the probability of a single debris impacting an AST. Based on this figure, the probability

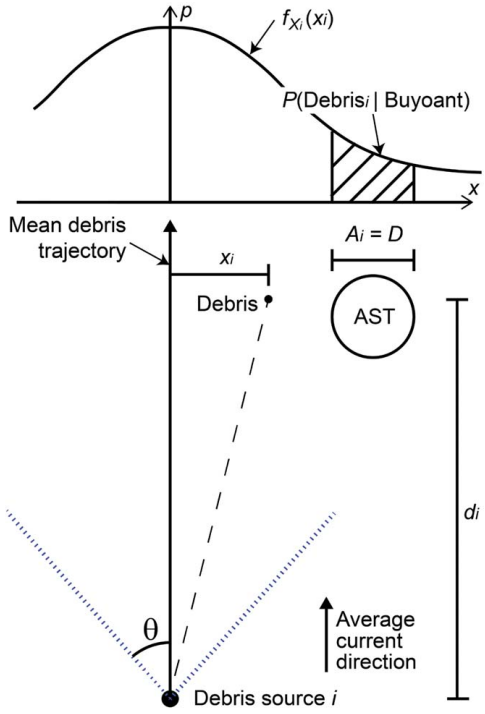


**Fig. 10.** Estimation of the probability of a debris impact.

that an already buoyant shipping container from debris source $i$ impacts a given AST is expressed as

$$P(\text{Debris}_i|\text{Buoyant}) = \int_{A_i} f_{X_i}(x_i)\,dx_i \tag{5}$$

where $A_i$ = the exposed area of the AST; $x_i$ = the lateral spreading of the debris; and $f_{Xi}(x_i)$ = the PDF of the lateral spreading. As a conservative assumption, the potential shielding effects of obstacles are neglected when evaluating Eq. (5) given the significant challenges associated with the determination of such effects. Stolle et al. (2018b) determined that the lateral spreading of shipping containers can be modeled as a normal distribution with a mean of 0 and a standard deviation $\sigma$, which is a function of the debris spreading angle ($\theta$) and the longitudinal displacement of the debris ($d_i$). As shown in Fig. 10, $\theta$ defines a circular sector where most debris would be transported from their source. Both Naito et al. (2014) and Nistor et al. (2017a) proposed definitions for $\theta$; however, this study adopts the value proposed by Naito et al. (2014) ($\theta = \pm 22.5°$), as it is obtained from empirical field observations rather than controlled experimental conditions. By adapting the approach of Stolle et al. (2018b), the standard deviation is defined as $\sigma = \tan(\theta/1.96)d_i$; $\theta$ is divided by 1.96 to ensure that 95% of the debris are within the spreading angle adopted here. It is acknowledged that the presence of obstacles and topographic features might affect the validity of the normal assumptions proposed by Stolle et al. (2018b). However, given the limited data available on debris motions, the consideration of this aspect is outside the scope of this study. By assuming that the nonstructural mass ($m_d$) of a shipping container is uniformly distributed with lower and upper bounds of 0 and $m_{\max}$, the probability that a shipping container from source $i$ becomes buoyant and then impacts a given AST is

$$\begin{aligned} P(\text{Debris}_i) &= P(\text{Debris}_i|\text{Buoyant}) \cdot P(\text{Buoyant}) \\ &= \frac{1}{m_{\max}} \int_{A_i} \int_0^{m_b} f_{X_i}(x_i) dm_d\, dx_i \end{aligned} \tag{6}$$

The number of shipping containers from all debris sources impacting an AST ($C$) can be expressed as

$$C = \sum_{i=1}^{I} \sum_{j=1}^{N_i} \mathbf{1}[\text{Debris}_i] \tag{7}$$

where $I$ = the number of debris sources; $N_i$ = the number of shipping containers in debris source $i$ and should be modeled as a random variable; and $\mathbf{1}[\text{Debris}_i]$ = a Bernoulli trial with probability of success $p_i = P(\text{Debris}_i)$ obtained from Eq. (6). The probability that at least one debris hits an AST is expressed as

$$P(C \geq 1) = 1 - P(C = 0) \tag{8}$$

Using the total probability theorem and the definition of a binomial distribution, the probability of having exactly zero debris impact is

$$P(C = 0) = \prod_{i=1}^{I} \sum_{n \in N_i} (1 - p_i)^n \cdot P(N_i = n) \tag{9}$$

where $n$ is summed over the domain of the discrete probability distribution of $N_i$. The number of shipping containers in a debris source is modeled here as discrete uniform distributions with lower bound $q_i$ and upper bound $r_i$. In this case, Eq. (9) reduces to

$$P(C = 0) = \prod_{i=1}^{I} \frac{1}{(r_i - q_i + 1)} \sum_{n=q_i}^{r_i} (1 - p_i)^n \tag{10}$$

Thus, to evaluate the probability of an AST being hit by shipping containers during a storm surge event [i.e., Eq. (8)] with above noted assumptions, $P(\text{Debris}_i)$ is the only unknown and can be estimated by evaluating Eq. (6) using numerical integration or Monte Carlo simulations (MCS). While this approach considers the potential for multiple debris impacts, Eqs. (7)–(10) assume that each debris impact is independent. It is acknowledged that this assumption might not be fully realistic, as shipping containers can move as an agglomeration (Nistor et al. 2017a); given a lack of data to characterize debris motions, this potential correlation between debris impacts is not considered here.

To consider the potential for damage due to debris impacts, the derived fragility models should be introduced in Eq. (6). Thus, the probability that a shipping container from debris source $i$ impacts and damages an AST is expressed as

$$P(\text{Damage}_i|\boldsymbol{\Theta_1}) = \frac{1}{m_{\max}} \int_{\boldsymbol{\Theta_2}} \int_{A_i} \int_{0}^{m_b} P(\text{Damage}_i|\boldsymbol{\Theta_1}, \boldsymbol{\theta_2}, y_d(x_i), m_d) \times f_{X_i}(x_i) f_{\boldsymbol{\Theta_2}}(\boldsymbol{\theta_2}) dm_d \cdot dx_i \cdot d\boldsymbol{\theta_2} \tag{11}$$

where $P(\text{Damage}_i|\boldsymbol{\Theta_1}, \boldsymbol{\theta_2}, y_d(x_i), m_d)$ = one of the three fragility models derived above, where the conditioning parameters (i.e., $\boldsymbol{IM_S}$, $\boldsymbol{IM_D}$, and $\boldsymbol{X}$) are regrouped differently for clarity; $\boldsymbol{\Theta_1}$ = the set of known conditioning parameters; $\boldsymbol{\Theta_2}$ = the set of uncertain parameters other than $y_d$ and $m_d$; and $f_{\boldsymbol{\Theta_2}}(\boldsymbol{\theta_2})$ = the joint probability distribution of the parameters in $\boldsymbol{\Theta_2}$. As shown in Eq. (11), the value of $y_d$ is determined directly from the lateral spreading. For illustration, only the tank shell damage fragility model with $\zeta_{pl1} = 0$ is employed for the risk assessment performed next. The geometry and design of ASTs are typically known before a storm and the surge conditions are assumed to be deterministic, leading to $\boldsymbol{\Theta_1} = \{D, H, S_d, S, U_w, H_w, T_w\}$. However, the exact contents and internal liquid levels of ASTs are usually unknown prior to a storm. Also, the debris impact conditions are uncertain, given the stochastic nature of debris motions, leading to $\boldsymbol{\Theta_2} = \{L, \rho_L, \alpha, \beta, U_d\}$. The uncertain parameters $L$, $\rho_L$, $\alpha$, and $\beta$ are modeled as uniform random variables with the lower and upper bounds shown in Tables 2 and 3. Based on Lin and Vanmarcke (2010), the nondimensional debris velocity (i.e., $U_d^* = U_d/U_w$) is modeled as a beta distribution with shape parameters $a = \bar{U}_d^* \eta$ and $b = (1 - \bar{U}_d^*)\eta$, where $\bar{U}_d^*$ and $\eta$ are, respectively, the mean and dispersion of $U_d^*$. For waterborne debris, $\bar{U}_d^*$ and $\eta$ can be expressed as (Stolle et al. 2018c)

$$\bar{U}_d^* = 1 - \left( \frac{C_d \rho_w A_d}{2 m_d} U_w t + 1 \right)^{-1} \tag{12}$$

$$\eta = \max\left( \frac{1}{\bar{U}_d^*}, \frac{1}{1 - \bar{U}_d^*} \right) + \gamma \tag{13}$$

where $C_d$ = the drag coefficient of the shipping container and taken as 1.05 (Stolle et al. 2017), $A_d$ = the submerged area of the shipping container projected toward the surge, $t$ = the travel time of the shipping container, and $\gamma$ = a free parameter that should be determined from empirical data and is assumed equal to 3 here (Lin and Vanmarcke 2010). Finally, with these assumptions, Eq. (11) can be evaluated using numerical integration or MCS, and the probability that at least one debris hits and damages an AST using Eqs. (8) and (10) with $p_i = P(\text{Damage}_i|\boldsymbol{\Theta_1})$ instead of $p_i = P(\text{Debris}_i)$.

Since the fragility models derived in this study do not consider the potential damage mechanisms related to storm surge loads alone, the framework presented above only indicate the probability of suffering damage following debris impacts, given that ASTs were not already damaged by surge loads alone (i.e., flotation and storm surge buckling). To obtain a comprehensive assessment of AST vulnerability, the above framework should be coupled with fragility models for storm surge failure, such as the one proposed by Bernier (2019). By assuming a series system (i.e., damage may occur due to storm surge alone or following debris impacts, whichever occurs first), the overall probability of damage is expressed as

$$P(\text{Damage}_{\text{Surge}} \cup \text{Damage}_{\text{Debris}}) = P(\text{Damage}_{\text{Surge}}) + P(\text{Damage}_{\text{Debris}}) - P(\text{Damage}_{\text{Surge}}) P(\text{Damage}_{\text{Debris}}) \tag{14}$$

where $P(\text{Damage}_{\text{Surge}})$ = the probability of damage due to storm surge loads alone, which can be computed according to Bernier (2019); and $P(\text{Damage}_{\text{Debris}})$ = the probability of damage following debris impacts, which can be evaluated using Eqs. (8) and (11). This equation relies on the fact that damage due to storm surge loads alone and damage following debris impacts are independent events. Since the debris impacts fragility models were derived for conditions that excluded the potential for damage mechanisms related to storm surge loads alone, these two events are independent.

### Case Study Application

To illustrate its application, the risk assessment framework is applied to a case study area located in the Houston region, in Texas, and for a deterministic storm surge scenario. Fig. 11 shows the case study area, which consists of a storage tank terminal located north of a shipping yard. This area is selected since a large concentration of shipping containers are located at a close distance to ASTs. Also, debris impacts are likely, given that the topography is almost flat and no major obstacle is present between the shipping containers and the ASTs. A total of seven debris sources are defined in the case study area [i.e., $I = 7$ in Eq. (7)]. Based on recent aerial

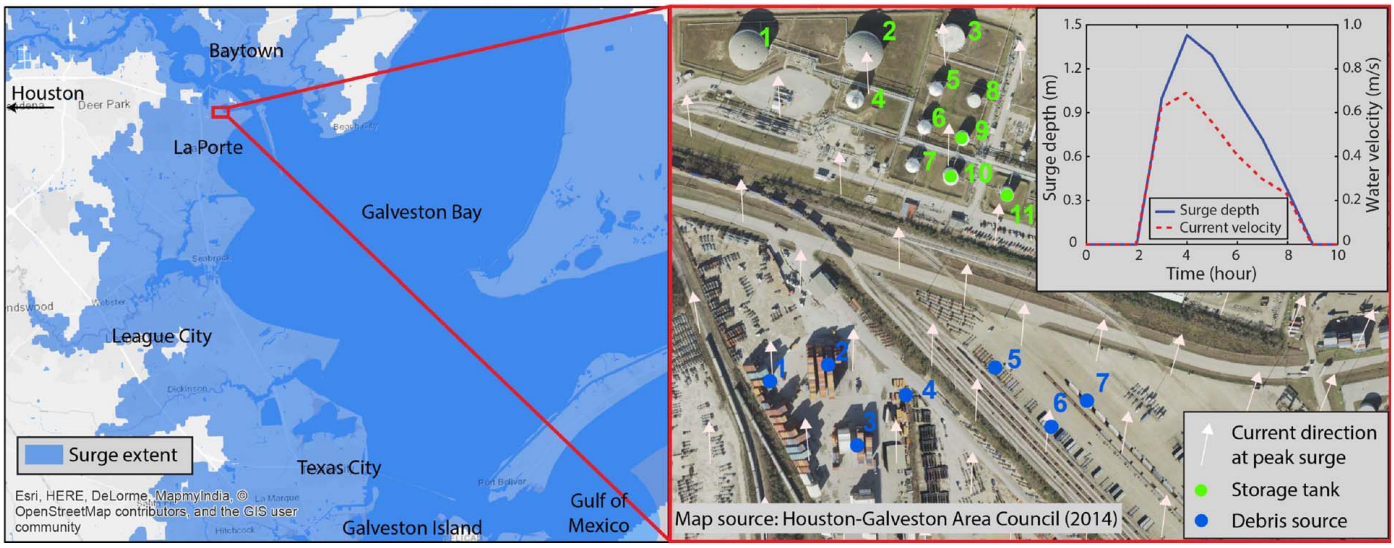


**Fig. 11.** Case study shipping yard and hydrodynamic conditions. (Base map from Esri, HERE, DeLorme, MapmyIndia, © OpenStreetMap contributors, and the GIS user community; Houston-Galveston Area Council 2014.)

**Table 4.** Number of shipping containers per debris source in the case study area

| Debris source (#) | Lower bound ($q_i$) | Upper bound ($r_i$) |
|---|---|---|
| 1, 2, 3, and 4 | 5 | 20 |
| 5, 6, and 7 | 0 | 10 |

**Table 5.** Dimensions of aboveground storage tanks in the case study area

| Storage tank (#) | Diameter (m) | Height (m) |
|---|---|---|
| 1 and 2 | 39.0 | 21.0 |
| 3 | 26.6 | 16.1 |
| 4 | 18.9 | 21.2 |
| 5, 6, and 7 | 15.2 | 15.8 |
| 8, 9, 10, and 11 | 13.9 | 11.5 |

imagery (Houston-Galveston Area Council 2014), Table 4 presents the lower and upper bounds (i.e., $q_i$ and $r_i$) for the number of shipping containers found at each location. Table 5 also presents the geometries of the eleven ASTs in the terminal, obtained from Bernier et al. (2017). To define the storm surge conditions in the area, the 500-year return period synthetic storm (i.e., Storm FEMA036) previously discussed is employed. This storm was developed by FEMA as part of its Flood Insurance Study of the Texas Coast and represents one of the most severe storm events that could hit the Houston region (Ebersole et al. 2016). Fig. 11 also shows the hydrodynamic conditions in the case study area, obtained from the *ADCIRC + SWAN* simulation previously discussed. At peak surge, the surge depth is 1.43 m and the current velocity is 0.67 m/s; due to the flat topography, these conditions are almost uniform across the area. The current direction at peak surge is also illustrated in Fig. 11. The *ADCIRC + SWAN* simulation also provides the values of $H_w$, and $T_w$ at the AST locations.

Figs. 12 and 13 present results of the risk assessment framework outlined for the case study area. Fig. 12(a) shows the probability of debris impacts for the eleven ASTs in the area using Eqs. (6) and (8), and Fig. 12(b) shows the probability of suffering damage due to debris impacts using Eqs. (8) and (11). The probabilities shown in Fig. 12 were computed using the peak surge and water velocity conditions shown in Fig. 11 and a $m_{\max}$ value of 28,300 kg, as in Table 2; for the surge conditions in the case study area, $m_b \approx 18{,}000$ kg. As mentioned earlier, shielding effects of obstacles are not taken into account when evaluating Eqs. (6) and (11). Fig. 12(a) indicates that all ASTs in the case study area have a probability of impacts of at least 50%. ASTs 1 and 2 have the highest probability of impacts (96% and 99%, respectively), given their larger size and larger $A_i$ when evaluating Eq. (6). Also, ASTs 1–7 have higher probability of impacts than do ASTs 8–11, given their alignment with debris sources containing a larger number of shipping containers (i.e., debris sources 1–4). Fig. 12(b) reinforces the findings observed in Fig. 7 regarding the effects of the diameter on the likelihood of damage. Despite having high probability of impacts, ASTs 1 and 2 have probability of damage less than 5%, given their large diameter. To a lesser extent, a similar behavior is observed for AST 3. All small ASTs (i.e., ASTs 4–11) have a probability of damage of at least 25%, and ASTs 7 and 10 have the highest probability of suffering damage (37% and 30%, respectively), given their direct alignment with debris sources 3 and 4.

Fig. 13 presents the overall probability of damage using Eq. (14) of the eleven ASTs in the case study area. To emphasize the relative importance of debris impacts, this figure also presents the probability of damage due to storm surge loads alone [i.e., $P(\text{Damage}_{\text{Surge}})$]. The probability of damage due to storm surge loads alone varies between 10% and 18%; taller ASTs have a smaller probability of damage due to the larger range of internal liquid level. As previously observed, the effects of debris are limited for large ASTs (i.e., ASTs 1 and 2); the vulnerability of these ASTs is driven by the storm surge effects. However, for small ASTs, debris impacts can have a significant influence on the overall probability of damage. In such cases, neglecting the potential for debris impacts can underestimate the probability of damage by 10% to 30% compared with the case where only storm surge loads are considered. Also, for ASTs 4–11, the contribution of debris impacts to the overall probability of damage is larger than the contribution of storm surge loads alone. Thus, ASTs that have a relatively small vulnerability to storm surge loads can become significantly more vulnerable due to the presence of and their exposure to waterborne debris. These results again highlight the importance of considering the effects of waterborne debris impacts, especially for ASTs located close to shipping yards or other debris sources.

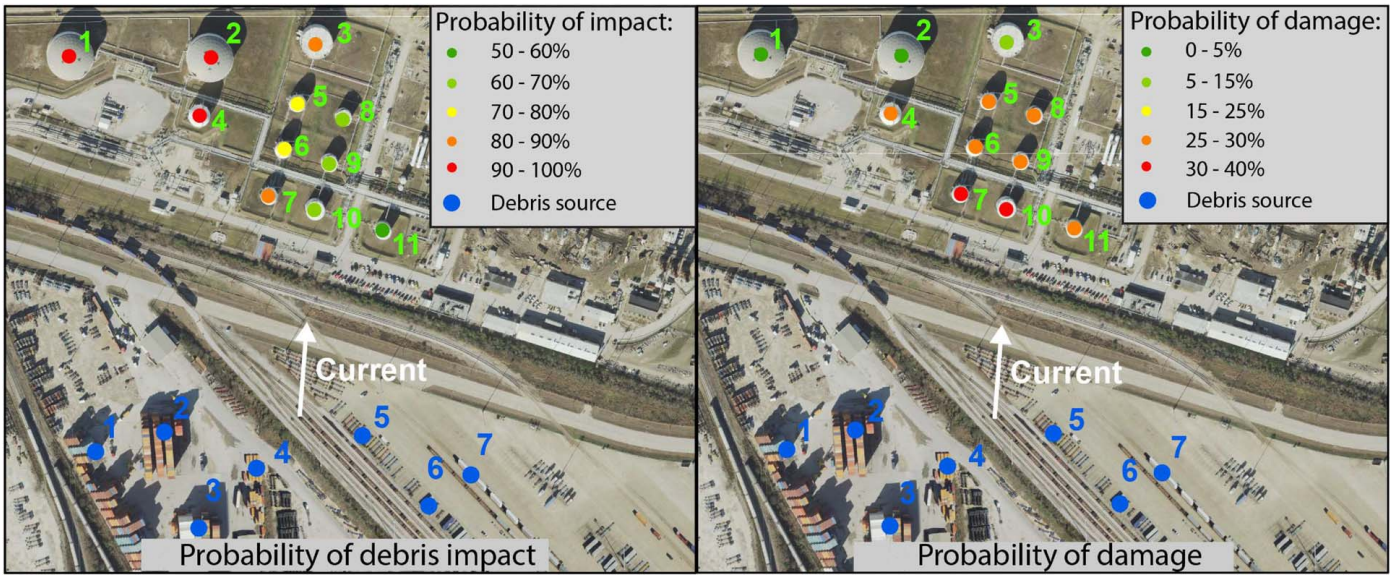


(a) (b)

**Fig. 12.** Results of the risk assessment: (a) probability of debris impacts; and (b) probability of AST damage due to debris impacts. (Base map from Houston-Galveston Area Council 2014.)

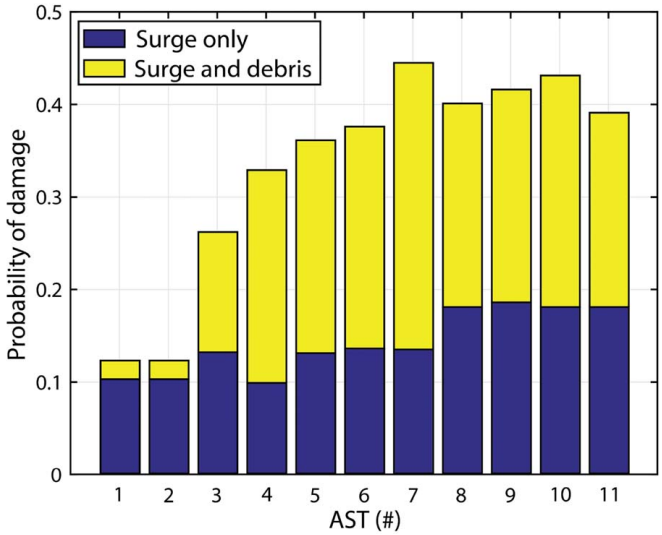


**Fig. 13.** Importance of debris impacts on the overall probability of damage.

### *Mitigation Strategies*

The fragility models and risk assessment framework proposed in this study are also useful tools to evaluate the viability of mitigation strategies. One of the preferred strategies to reduce the vulnerability of ASTs consists of filling them to increase their self-weight and resistance against lateral loads. Storm preparation guides recommend completely filling ASTs or, if not possible, filling them with liquid at least 0.9–1.8 m above the expected surge level (EPA 2016). While the viability of such measures has been confirmed for ASTs subjected to storm surge loads alone (Bernier et al. 2018), their effectiveness for ASTs subjected to waterborne debris impact is investigated here for the first time.

Fig. 14 shows the effects of varying the internal liquid level on the vulnerability of the ASTs in the case study area. Fig. 14(a) presents fragility curves obtained from Eq. (4) for AST 7, and Fig. 14(b) presents the overall probability of damage obtained from Eq. (14) for all ASTs in the case study area. The fragility curves in Fig. 14(a) are for tank shell damage with $\zeta_{pl1} = 0$, are conditioned on $m_d$, and are obtained for the hydrodynamic conditions in the case study area (i.e., $S = 1.43$ m and $U_w = U_d = 0.67$ m/s); all other parameters are uniformly distributed with the bounds shown in Tables 2 and 3. As a reminder, the fragility curves in Fig. 14(a) only consider the potential for damage due to debris impacts, contrary to Fig. 14(b) which also accounts for storm surge-related damage mechanisms (i.e., flotation and buckling). Results in Fig. 14(a) indicate that an internal liquid 1.8 m above the surge level has a limited effect on the fragility of AST 7, whereas completely filling this AST can reduce the probability of tank shell damage due to debris impacts by up to 30%. However, even if the AST is completely filled, high probabilities of damage can still be observed in case of impacts with debris having a large nonstructural mass. Fig. 14(b) shows that filling ASTs in the case study area 1.8 m above the surge height can significantly reduce the overall probability of damage of the ASTs, since this measure eliminates the potential for flotation or storm surge buckling; the ASTs are now only vulnerable to debris impacts. Anchoring the ASTs to the ground, another potential mitigation strategy, would result in almost identical vulnerability levels. Again, completely filling the ASTs can further reduce the overall probability of damage due to a larger internal pressure resisting the impact loads, but some ASTs in the case study area still exhibit relatively large probability of damage. In the case of sliding, additional analyses not shown in Fig. 14 indicate that completely filling the ASTs provide a sufficient self-weight to eliminate the potential for sliding. Overall, these results indicate that while filling ASTs prior to a storm can significantly reduce the likelihood of storm surge-related failures and sliding, the effects are limited to protect ASTs against tank shell damage following debris impacts. Moreover, in the case of severe damage to the tank shell that leads to a rupture, the consequences would be significantly higher, given the larger volume of liquid to spill. Thus, filling ASTs might not be an optimal strategy to reduce the vulnerability of ASTs located near debris sources, and additional mitigation strategy, such as modifying the tank stiffness, should be investigated.

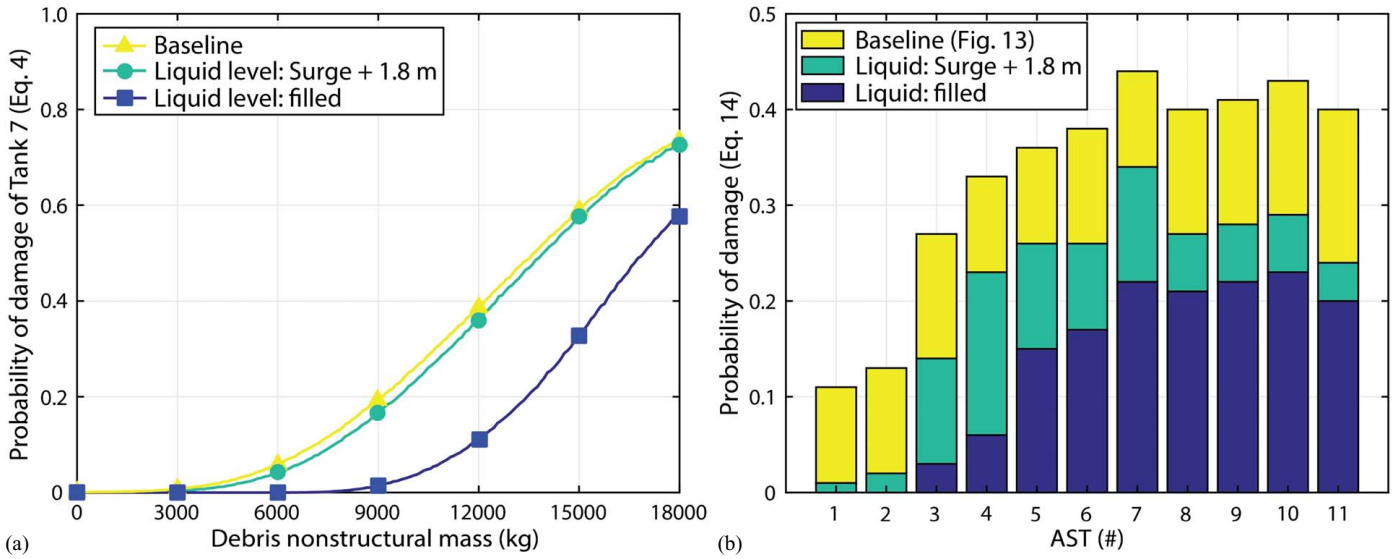


**Fig. 14.** Effects of varying internal liquid height on: (a) fragility curve [Eq. (4)] of tank #7; and (b) overall probability of damage [Eq. (14)] of ASTs in the case study area.

## Discussion and Future Work

This study offers the first fragility models and risk assessment framework for ASTs exposed to waterborne debris during storm events. However, the development of these tools relied on several assumptions, and future work is required to address the limitations posed by these assumptions. First, the fragility models were developed using numerical simulations, and several modeling assumptions were not comprehensively validated. This limited validation results in FE models with potentially large uncertainties and modeling errors, which, in turn, can affect the performance of the fragility models. One major assumption potentially affecting the performance of the developed models is the added mass of the debris, which was not considered here. While the comparison presented in Riggs et al. (2014) between in-air and in-water impact tests of a scaled 20-ft shipping container indicates that hydrodynamic effects do not significantly affect impact loads, other experiments performed by Shafiei et al. (2016) show that they can substantially amplify impact loads, depending on the debris draft, orientation, and flow conditions. Moreover, recent experiments indicate that hydrodynamic conditions around a structure can also affect the debris velocity, eccentricity, and orientation right before impact (Derschum et al. 2018). Thus, future investigations are required to better understand the importance of interactions between the debris, fluid, and structure on the behavior and vulnerability of ASTs. It is worth mentioning that the parametrization of the fragility models derived here offers some flexibility to consider hydrodynamic and added mass effects by modifying $m_d$, $U_d$, $\alpha$, $\beta$, and $y_d$ accordingly; however, such an approach would still require validation.

Another modeling assumption that requires further investigation is the nonstructural mass of the shipping container. Numerical work presented by Piran Aghl et al. (2015b) indicates that rigidly attaching the nonstructural mass, as in this study, can overestimate the impact loads, compared with cases where the nonstructural mass is allowed to slide or is attached to the container using linear springs and dampers. While Piran Aghl et al. (2015b) proposed some values to define the springs, dampers, or friction between the mass and container floor based on experiments, these values were obtained from idealized systems. Given the large variety of content in shipping containers and systems to secure this content, additional work is required to adequately model and define the uncertainties associated with the connectivity between the nonstructural mass and the shipping container.

Furthermore, while the fragility models developed here provide the likelihood of damage of an AST, they do not necessarily indicate the likelihood of a loss of containment (i.e., release of the internal liquid). Since the major consequences of an AST failure are related to the loss of containment, comprehensive risk assessment should also quantify the likelihood of such an event (Caputo et al. 2018), and future research is required to define limit states and damage levels that can actually predict loss of containment rather than only the occurrence of inelastic damage or sliding.

The risk assessment framework developed in the previous section also relied on major assumptions obtained from limited field investigations as well as idealized and small-scale experiments. Therefore, as additional experimental and empirical data and modeling tools become available, several assumptions should be validated or improved. This includes the: (1) adequacy of employing results obtained from tsunami hydrodynamic conditions for storm surge conditions; (2) validity, at full scale, of results derived from relatively small-scale experiments (Stolle et al. 2018b); (3) validity of the spreading normal distribution and velocity beta distribution for debris traveling over complex landscapes, such as industrial complexes; (4) need to model the potential correlation between multiple debris impacts; and (5) need to consider the shielding and flow velocity amplification caused by obstacles (Hatzikyriakou and Lin 2017; Nouri et al. 2010) when evaluating risks. Lastly, the failure of ASTs during storm events can also result in cascading impacts (or domino effects) since a floating or sliding AST can become a debris and impact other surrounding ASTs. Moreover, within an industrial complex, waterborne debris could damage infrastructures other than ASTs, potentially generating additional debris. Since capturing such cascading effects can be essential to obtain adequate measure of risk and vulnerability in coastal regions (Hatzikyriakou and Lin 2017), future studies could further adapt the framework developed here to consider cascading impacts.

Despite the limitations listed here, the tools, models, and methods developed as part of this study represent a major advancement

to better understand, evaluate, and mitigate the vulnerability of ASTs during storms events, and also open the path for future research across fields of coastal engineering.

## Conclusions

This paper aimed to develop a methodology to explore the structural behavior and vulnerability of ASTs subjected to waterborne debris impacts during storm surge events. First, FE models of ASTs and of a shipping container were developed to perform debris impact analysis. The shipping container model was also validated against experimental results available in the literature. Simulation-based fragility models were then derived for two damage mechanisms: (1) damage to the tank shell and (2) sliding of the ASTs. To facilitate their future adoption or implementation, the fragility models were parametrized on modeling and load parameters so that they can be used to readily assess the vulnerability of ASTs subjected to a range of realistic surge and debris impact conditions. Since the derived fragility models were conditioned on the occurrence of debris impacts, this study also presented a framework to assess the probability of shipping containers impacting ASTs and then use the fragility models to evaluate and mitigate the risks posed to ASTs by waterborne debris during storm events. The risk assessment framework was applied to a case study storage terminal in the Houston, Texas, region. Results of the fragility and risk assessments provided the following insights:

- Debris impacts can be of paramount importance to assess the structural vulnerability of ASTs located near debris sources during storm surge events. Neglecting debris impacts can significantly underestimate the probability of damage.
- Large-diameter ASTs are less likely to suffer damage following a debris impact than are small-diameter ASTs. Damage mechanisms related to storm surge loads alone (i.e., flotation and storm surge buckling) are more critical for large ASTs.
- The debris velocity and nonstructural mass have the largest influence on the likelihood of damage. Debris orientation and eccentricity also have a nonnegligible effect on the likelihood of damage, as these parameters determine how the debris bounces off the AST.
- Damage to the tank shell is the dominant damage mechanism, compared with sliding.
- Filling ASTs with liquid prior to a storm has a limited effect in reducing the vulnerability of ASTs subjected to debris impact and might not be an optimal mitigation measure.

Overall, this study represents a first step to better understanding the vulnerability of ASTs during severe storm events and offers useful tools and methods to perform basic screening studies of vulnerable ASTs in port and industrial regions. Furthermore, as long as sufficient information is available, the tools and methods developed here can be adapted to other infrastructure beyond ASTs, other debris types besides shipping containers, and other hydrodynamic conditions than storm surge. Nonetheless, while this study offers a good starting point to assess the risks posed by waterborne debris, future improvements are still required to better capture the complexities associated with debris motions and impacts in coastal regions.

## Data Availability Statement

Some or all data, models, or code used during the study were provided by a third party (*ADCIRC + SWAN* simulation results). Direct requests for these materials may be made to the provider, as indicated in the Acknowledgements.

Some or all data, models, or code generated or used during the study are available from the corresponding author by request (Shipping container finite-element model; Aboveground storage tank finite-element model; Artificial Neural Network to estimate wave loads; Matlab code to generate Latin Hypercube samples; and Matlab code to perform risk assessment).

## Acknowledgments

The authors acknowledge the support of this research by the National Science Foundation under award CMMI-1635784. The first author was also supported in part by the Natural Sciences and Engineering Research Council of Canada. The authors thank Prof. Clint Dawson (University of Texas at Austin) for providing the *ADCIRC + SWAN* data. Any opinions, findings, and conclusions or recommendations expressed herein are those of the authors and do not necessarily reflect the views of the sponsors.

## Supplemental Data

Tables S1–S4 are available online in the ASCE Library (www.ascelibrary.org).

## References

API (American Petroleum Institute). 2013. *Welded tanks for oil storage*. API Standard 650. Washington, DC: API.

Bernier, C. 2019. "Fragility and risk assessment of aboveground storage tanks during storm events." Ph.D. thesis, Dept. of Civil and Environmental Engineering, Rice Univ.

Bernier, C., J. R. Elliott, J. E. Padgett, F. Kellerman, and P. B. Bedient. 2017. "Evolution of social vulnerability and risks of chemical spills during storm surge along the Houston Ship Channel." *Nat. Hazard. Rev.* 18 (4): 04017013. https://doi.org/10.1061/(ASCE)NH.1527-6996.0000252.

Bernier, C., S. Kameshwar, J. R. Elliott, J. E. Padgett, and P. B. Bedient. 2018. "Mitigation strategies to protect petrochemical infrastructure and nearby communities during storm surge." *Nat. Hazard. Rev.* 19 (4): 04018019. https://doi.org/10.1061/(ASCE)NH.1527-6996.0000309.

Bernier, C., and J. E. Padgett. 2019. "Neural networks for estimating storm surge loads on storage tanks." In *Proc., 13th Int. Conf. on Applications of Statistics and Probability in Civil Engineering*. Seoul: Seoul National University.

Caputo, A. C., F. Paolacci, O. S. Bursi, and R. Giannini. 2019. "Problems and perspectives in seismic quantitative risk analysis of chemical process plants." *J. Pressure Vessel Technol.* 141 (1): 010901.

Charvet, I., A. Suppasri, H. Kimura, D. Sugawara, and F. Imamura. 2015. "A multivariate generalized linear tsunami fragility model for Kesennuma City based on maximum flow depths, velocities and debris impact, with evaluation of predictive accuracy." *Nat. Hazards* 79 (3): 2073–2099.

Como, A., and H. Mahmoud. 2013. "Numerical evaluation of tsunami debris impact loading on wooden structural walls." *Eng. Struct.* 56: 1249–1261.

Containex. 2013. "Technical specifications for steel dry cargo container 20′×8′×8′6″ ISO 1CC type." Accessed August 18, 2018. http://www.containex.com/en/products/shipping-container.

Cowper, G. R., and P. S. Symonds. 1957. *Strain-hardening and strain-rate effects in the impact loading of cantilever beams*. Providence, RI: Division of Applied Mathematics, Brown Univ.

Cozzani, V., M. Campedel, E. Renni, and E. Krausmann. 2010. "Industrial accidents triggered by flood events: Analysis of past accidents." *J. Hazard. Mater.* 175 (1–3): 501–509.

Derschum, C., I. Nistor, J. Stolle, and N. Goseberg. 2018. "Debris impact under extreme hydrodynamic conditions part 1: Hydrodynamics and impact geometry." *Coastal Eng.* 141: 24–35.

Ebersole, B. A., T. C. Massey, J. A. Melby, N. C. Nadal-Caraballo, D. L. Hendon, T. W. Richardson, and R. W. Whalin. 2016. *Interim report—Ike Dike concept for reducing hurricane storm surge in the Houston-Galveston region*. Jackson, MS: Jackson State Univ.

Eligehausen, R., R. Mallee, and J. F. Silva. 2006. *Anchorage in concrete construction*. Berlin: Wiley.

EPA (Environmental Protection Agency). 2016. *RRT6 fact sheet #103a: Flood preparedness recommended best practices*. Dallas, TX: EPA.

Godoy, L. 2007. "Performance of storage tanks in oil facilities damaged by Hurricanes Katrina and Rita." *J. Perform. Constr. Facil.* 21 (6): 441–449. https://doi.org/10.1061/(ASCE)0887-3828(2007)21:6(441).

Hatzikyriakou, A., and N. Lin. 2017. "Impact of performance interdependencies on structural vulnerability: A systems perspective of storm surge risk to coastal residential communities." *Reliab. Eng. Syst. Saf.* 158: 106–116.

Hatzikyriakou, A., N. Lin, J. Gong, S. Xian, X. Hu, and A. Kennedy. 2016. "Component-Based vulnerability analysis for residential structures subjected to storm surge impact from Hurricane Sandy." *Nat. Hazard. Rev.* 17 (1): 05015005. https://doi.org/10.1061/(ASCE)NH.1527-6996.0000205.

Herbin, A. H., and M. Barbato. 2012. "Fragility curves for building envelope components subject to windborne debris impact." *J. Wind Eng. Ind. Aerodyn.* 107–108: 285–298.

Houston-Galveston Area Council. 2014. "Aerial and LiDAR Imagery." Accessed January 27, 2016. http://www.h-gac.com/imagery/default.aspx.

Kameshwar, S., and J. E. Padgett. 2016. "Stochastic modeling of geometric imperfections in aboveground storage tanks for probabilistic buckling capacity estimation." *ASCE-ASME J. Risk Uncertain. Eng. Syst. Part A: Civ. Eng.* 2 (2): C4015005.

Kameshwar, S., and J. E. Padgett. 2018. "Fragility and resilience indicators for portfolio of Oil storage tanks subjected to hurricanes." *J. Infrastruct. Syst.* 24 (2): 04018003. https://doi.org/10.1061/(ASCE)IS.1943-555X.0000418.

Krausmann, E., and F. Mushtaq. 2008. "A qualitative Natech damage scale for the impact of floods on selected industrial facilities." *Nat. Hazards* 46 (2): 179–197.

Landucci, G., G. Antonioni, A. Tugnoli, and V. Cozzani. 2012. "Release of hazardous substances in flood events: Damage model for atmospheric storage tanks." *Reliab. Eng. Syst. Saf.* 106: 200–216.

Leonards, G. A. 1965. *Experimental study of static and dynamic friction between soil and typical construction materials*. Lafayette, IN: Purdue University.

Lin, N., and E. Vanmarcke. 2010. "Windborne debris risk analysis—Part I. Introduction and methodology." *Wind Struct.* 13 (2): 191–206.

Madurapperuma, M. A. K. M., and A. C. Wijeyewickrema. 2013. "Response of reinforced concrete columns impacted by tsunami dispersed 20′ and 40′ shipping containers." *Eng. Struct.* 56: 1631–1644.

Mckay, M. D., R. J. Beckman, and W. J. Conover. 1979. "A comparison of three methods for selecting values of input variables in the analysis of output from a computer code." *Technometrics* 21 (2): 239–245.

Naito, C., C. Cercone, H. R. Riggs, and D. Cox. 2014. "Procedure for site assessment of the potential for tsunami debris impact." *J. Waterway, Port, Coastal, Ocean Eng.* 140 (2): 223–232. https://doi.org/10.1061/(ASCE)WW.1943-5460.0000222.

Naito, C., D. Cox, Q. K. Yu, and H. Brooker. 2013. "Fuel storage container performance during the 2011 Tohoku, Japan, Tsunami." *J. Perform. Constr. Facil.* 27 (4): 373–380. https://doi.org/10.1061/(ASCE)CF.1943-5509.0000339.

Nistor, I., N. Goseberg, J. Stolle, T. Mikami, T. Shibayama, R. Nakamura, and S. Matsuba. 2017a. "Experimental investigations of debris dynamics over a horizontal plane." *J. Waterway, Port, Coastal, Ocean Eng.* 143 (3): 04016022. https://doi.org/10.1061/(ASCE)WW.1943-5460.0000371.

Nistor, I., N. Goseberg, and J. Stolle. 2017b. "Tsunami-driven debris motion and loads: A critical review." *Front. Built Environ.* 3: 1–11.

Nouri, Y., I. Nistor, D. A. N. Palermo, and A. Cornett. 2010. "Experimental investigation of tsunami impact on free standing structures." *Coastal Eng. J.* 52 (1): 43–70.

Paultre, P. 2011. *Dynamics of structures*. Hoboken, NJ: John Wiley & Sons.

Piran Aghl, P., C. J. Naito, and H. R. Riggs. 2014. "Full-Scale experimental study of impact demands resulting from high mass, Low velocity debris." *J. Struct. Eng.* 140 (5): 04014006. https://doi.org/10.1061/(ASCE)ST.1943-541X.0000948.

Piran Aghl, P., C. J. Naito, and H. R. Riggs. 2015a. "Estimation of demands resulting from inelastic axial impact of steel debris." *Eng. Struct.* 82: 11–21.

Piran Aghl, P., C. J. Naito, and H. R. Riggs. 2015b. "Effect of nonstructural mass on debris impact demands: Experimental and simulation studies." *Eng. Struct.* 88: 163–175.

Rabbat, B. G., and H. G. Russell. 1985. "Friction coefficient of steel on concrete or grout." *J. Struct. Eng.* 111 (3): 505–515. https://doi.org/10.1061/(ASCE)0733-9445(1985)111:3(505).

Riggs, H. R., D. T. Cox, C. J. Naito, M. H. Kobayashi, P. Piran Aghl, H. T.-S. Ko, and E. Khowitar. 2014. "Experimental and analytical study of water-driven debris impact forces on structures." *J. Offshore Mech. Arct. Eng.* 136 (4): 041603.

Robertson, I. N., H. R. Riggs, S. C. Yim, and Y. L. Young. 2007. "Lessons from Hurricane Katrina storm surge on bridges and buildings." *J. Waterway, Port, Coastal, Ocean Eng.* 133 (6): 463–483. https://doi.org/10.1061/(ASCE)0733-950X(2007)133:6(463).

Sengul, H., N. Santella, L. J. Steinberg, and A. M. Cruz. 2012. "Analysis of hazardous material releases due to natural hazards in the United States." *Disasters* 36 (4): 723–743.

Shafiei, S., B. W. Melville, A. Y. Shamseldin, K. N. Adams, and S. Beskhyroun. 2016. "Experimental investigation of tsunami-borne debris impact force on structures: Factors affecting impulse-momentum formula." *Ocean Eng.* 127: 158–169.

Stolle, J., C. Derschum, N. Goseberg, I. Nistor, and E. Petriu. 2018a. "Debris impact under extreme hydrodynamic conditions part 2: Impact force responses for non-rigid debris collisions." *Coastal Eng.* 141: 107–118.

Stolle, J., N. Goseberg, I. Nistor, and E. Petriu. 2018b. "Probabilistic investigation and risk assessment of debris transport in extreme hydrodynamic conditions." *J. Waterway, Port, Coastal, Ocean Eng.* 144 (1): 04017039. https://doi.org/10.1061/(ASCE)WW.1943-5460.0000428.

Stolle, J., N. Goseberg, I. Nistor, and E. Petriu. 2019. "Debris impact forces on flexible structures in extreme hydrodynamic conditions." *J. Fluids Struct.* 84: 391–407.

Stolle, J., I. Nistor, N. Goseberg, T. Mikami, and T. Shibayama. 2017. "Entrainment and transport dynamics of shipping containers in extreme hydrodynamic conditions." *Coastal Eng. J.* 59 (03): 1750011.

Stolle, J., I. Nistor, N. Goseberg, and E. Petriu. 2018c. "Probabilistic investigation of debris impact velocities during extreme flooding events." In *Proc., 36th International Conference on Coastal Engineering*. Reston, VA: ASCE.

USACE (United States Army Corps of Engineers). 2008. *Coastal engineering manual—Part II*. Washington, DC: USACE.